Supporting Information

Photo-electrical Properties of 2D Quantum Confined Metal Organic Chalcogenides Nanocrystal Films

Lorenzo Maserati[†§], Mirko Prato[¶], Stefano Pecorario[†‡], Bianca Passarella[†⊥], Andrea Perinot[†], Anupa Anna Thomas[†▽], Filippo Melloni[†‡], Dario Natali[⊥†] and Mario Caironi[†]**

[†] Center for Nano Science and Technology @PoliMi, Istituto Italiano di Tecnologia, 20133 Milan, Italy.

[§] The Molecular Foundry, Lawrence Berkeley National Laboratory, Berkeley, CA 94720, USA.

[¶] Materials Characterization Facility, Istituto Italiano di Tecnologia, 16163 Genova, Italy.

[‡] Department of Energy, Politecnico di Milano, 20156 Milan, Italy.

[⊥] Department of Electronics, Information and Bioengineering, Politecnico di Milano, 20133 Milan, Italy

[▽] Department of Physics, Politecnico di Milano, 20133 Milan, Italy.

* Correspondence to: lorenzo.maserati@iit.it, mario.caironi@iit.it

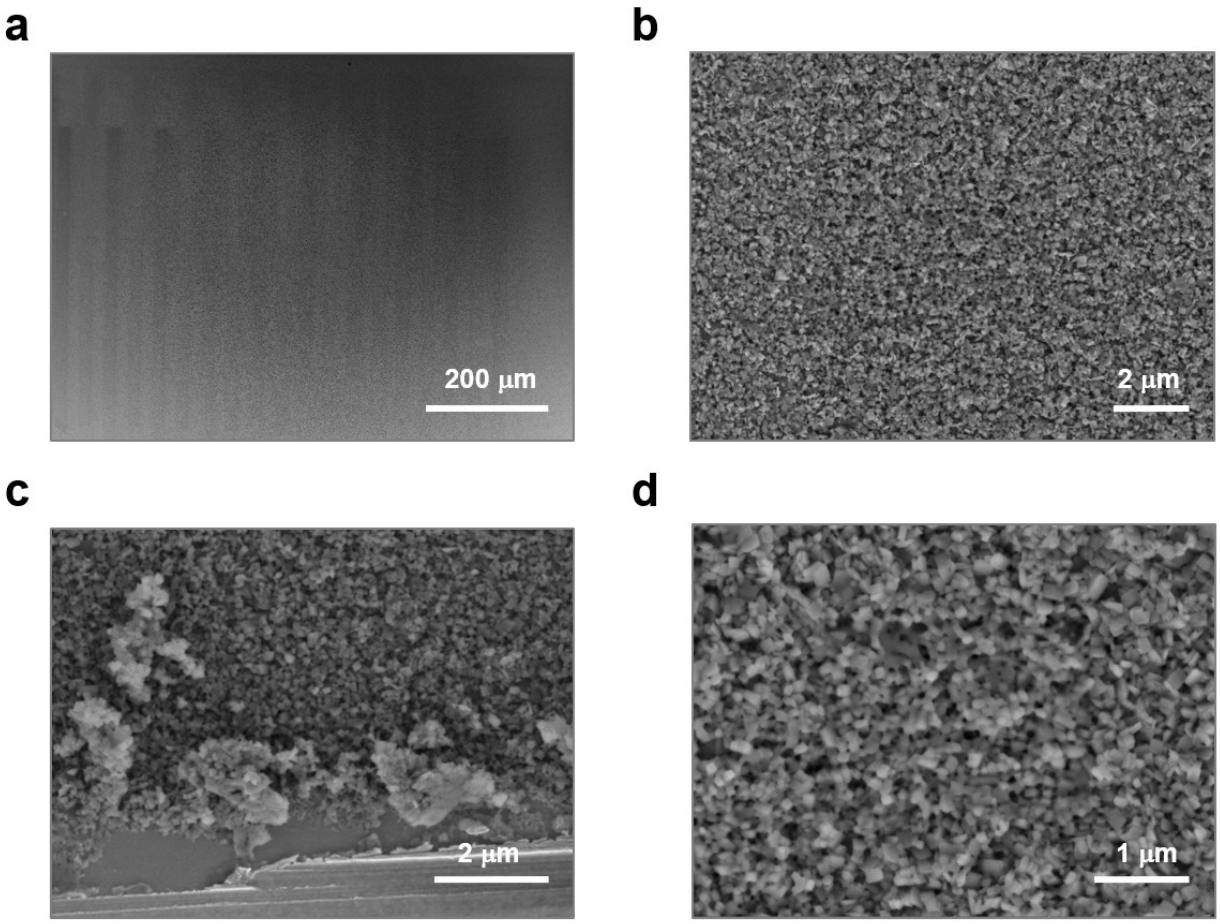

Figure S1 a-d, Scanning electron microscopy (SEM) imaging of the devices used for the electrical characterization of the nanocrystal (NC) films.

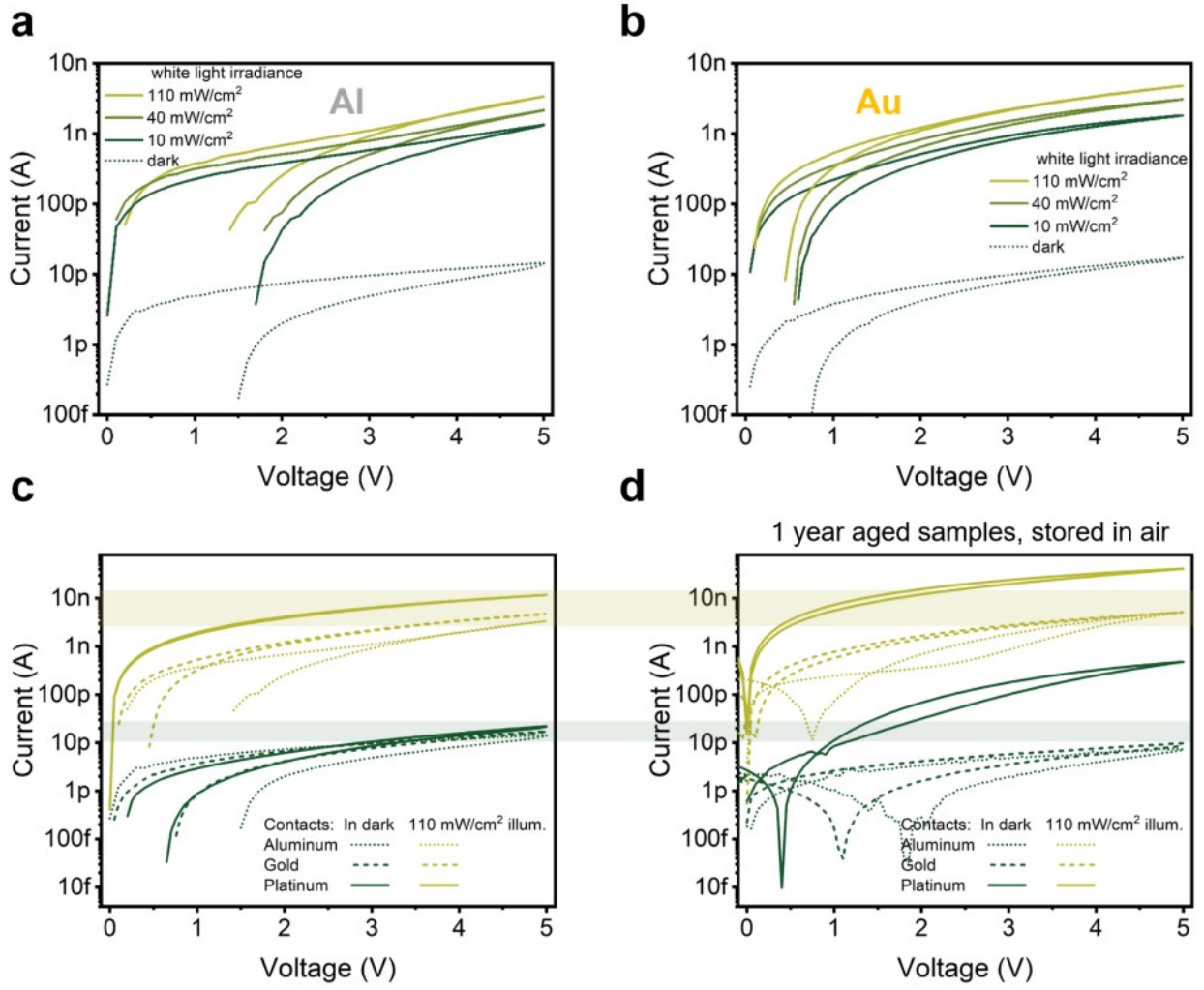

Figure S2. NC films electrical characteristics using different metal contacts. **a-b,** IV curves in dark (dashed lined) and under different white light illuminations (green solid lines) for aluminium **(a)** and gold **(b)** contacts, respectively. Panel **(c)** compares directly the dark and photo- current of the NC films with three different metal contacts: aluminium (dotted lines), gold (dashed lines), platinum (solid lines) under dark (dark green lines) and white light illumination (light green lines). Platinum contacts give the highest photocurrent and the smallest hysteresis in dark currents. Nevertheless, upon aging in standard lab environment conditions, platinum contacts behaviour changes over the weeks; on the other hand devices fabricated with aluminium and gold contacts show unaltered performances after 1 year **(d)** – shaded bars are guides for the eyes.

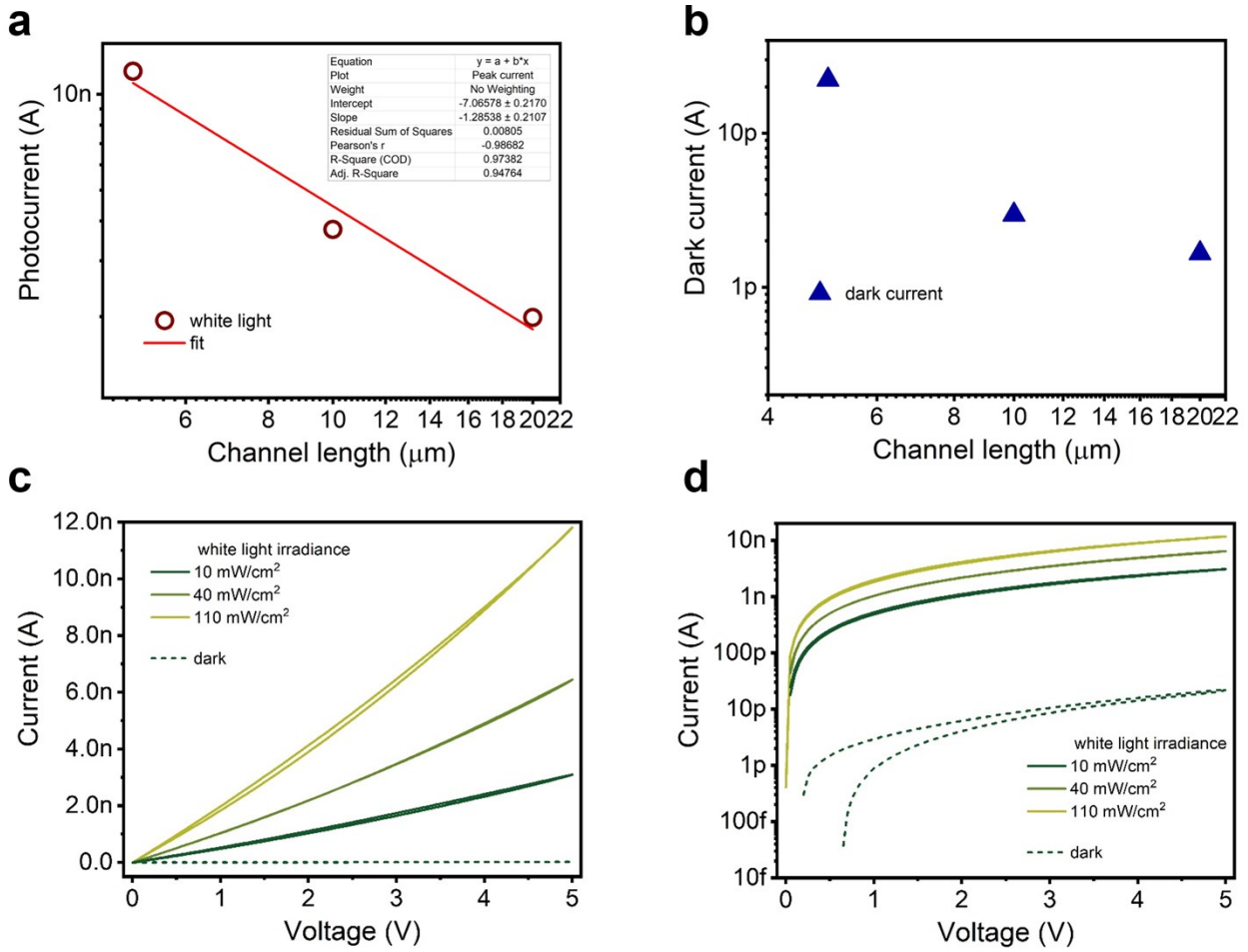

Figure S3. a, Channel length effect on dark and photocurrent shown in log-log plot current vs channel length (white light irradiance ~110 mW/cm^2, platinum electrodes). While the dark current scaling does not follow simple exponential or power laws, the photo-generated current scales with $1/L^{1.29}$. **c-d,** Current vs. voltage (IV) curves of the 5 μm-channel, platinum contacts, obtained with different illumination irradiances (~10, ~40, ~110 mW/cm^2, represented in dark green, green, light green, respectively) , plotted in linear **(c)**, and semi-logarithmic **(d)** scales.

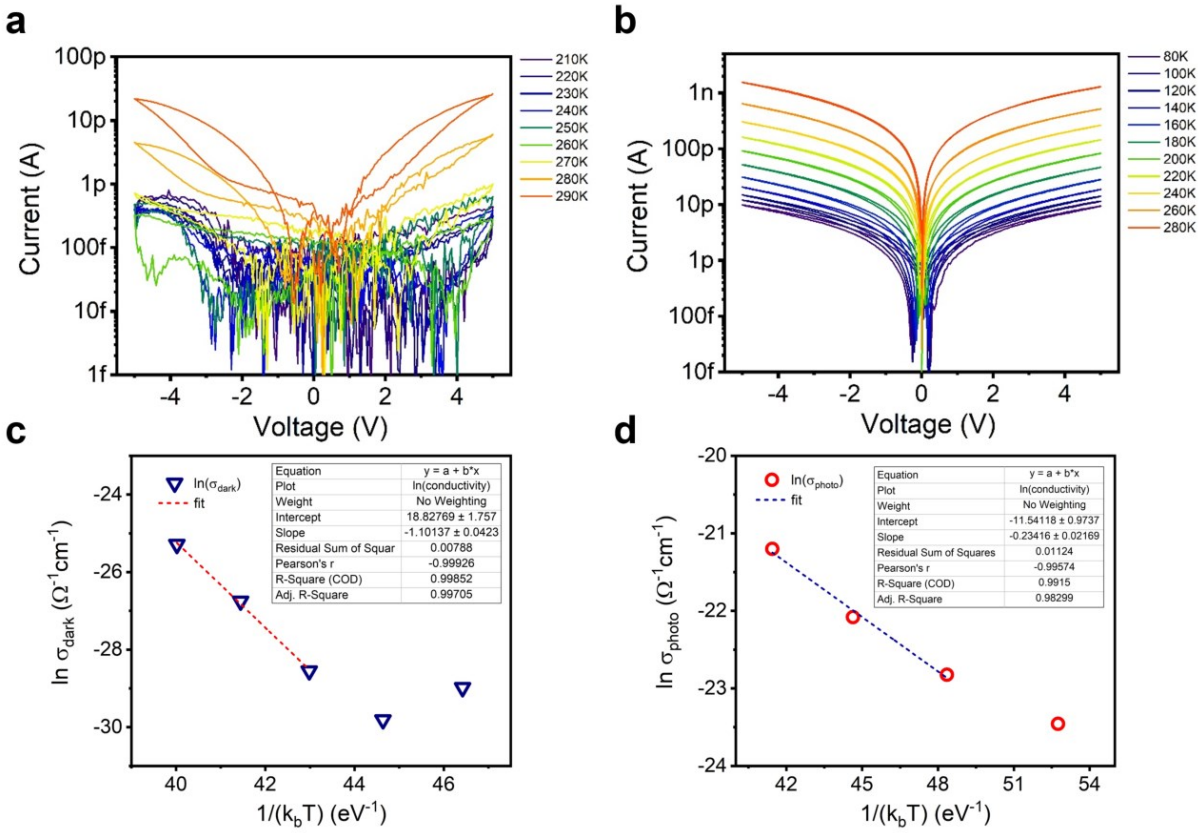

Figure S4. IV curves at different temperatures for 5 μm channel. In dark conditions **(a)** and under white light illumination **(b)**, with platinum electrodes. The current maxima are reported in the main text Fig. 3d. **c-d,** Semi-log plot showing an Arrhenius-type behaviour of the dark conductivity **(c)** and photo-conductivity **(d)** [$\sigma(T) = \sigma_0 e^{E_A/k_B T}$]. This is cast against the inverse of the thermal energy expressed in k_b units to highlight the activation energy of the charge carriers transport (represented by the fit slope), which is E_A = 1.10 eV in dark conditions and E_A = 0.23 eV under white light. The fits are taken on the highest temperature data points for dark current instrumental sensitivity constraints and for comparing the photocurrent thermal activation to the same data range.

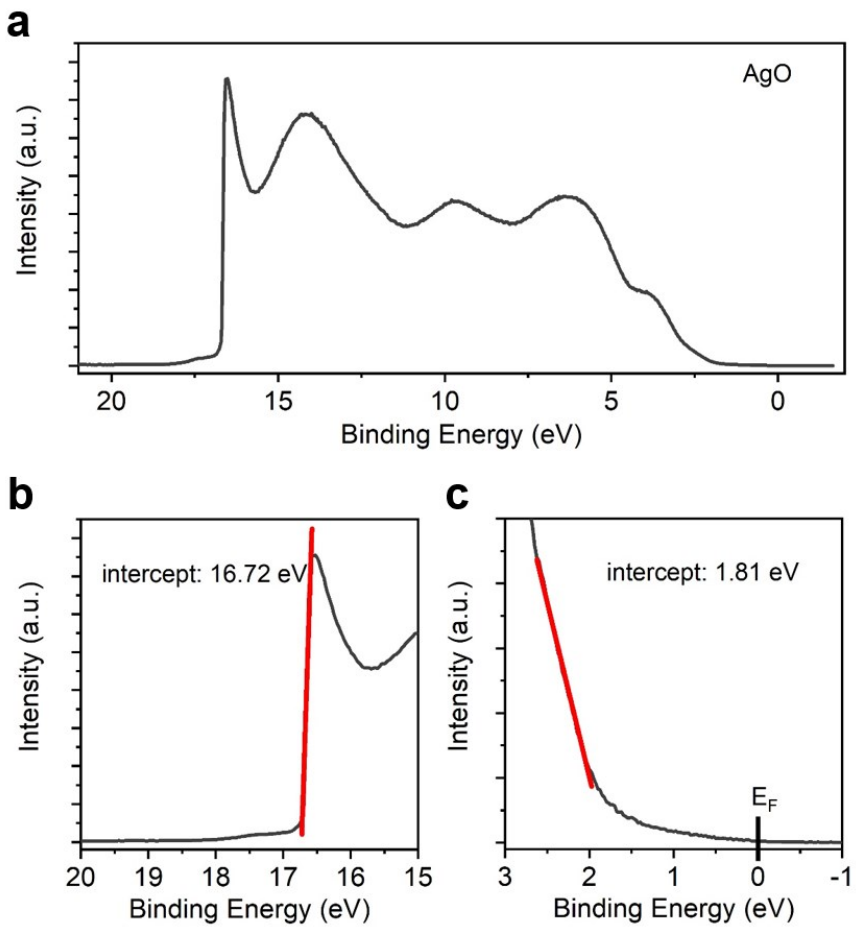

Figure S5. Semiconducting behaviour of AgO distinct from $[AgSePh]_{\infty}$. a, Photo-emitted electrons data. **b-c**, Zoomed inset of **(a)**. The work function is calculated by extracting the position of the high binding energy onset. Here the onset is at 16.72 eV (b). The photon energy used in the experiment is 21.22 eV. We could therefore write: WF = (21.22 – 16.72) eV = 4.5 eV. To extract the position of the valence band maximum (VBM) with respect to vacuum level, first the position of the low binding energy onset has to be determined. In the present case we consider as onset the steep raise of the signal at approx. 2 eV. By linear extrapolation, we obtained an intercept at 1.81 eV. Note: there is still signal below 2 eV and we could also consider the slowly raising slope that goes down to the Fermi level, at 0 eV of binding energy. Under these assumptions, the VBM is at ~1.8 eV below Fermi, meaning that it is at: (1.81 + 4.5) eV = 6.31 eV below vacuum level.

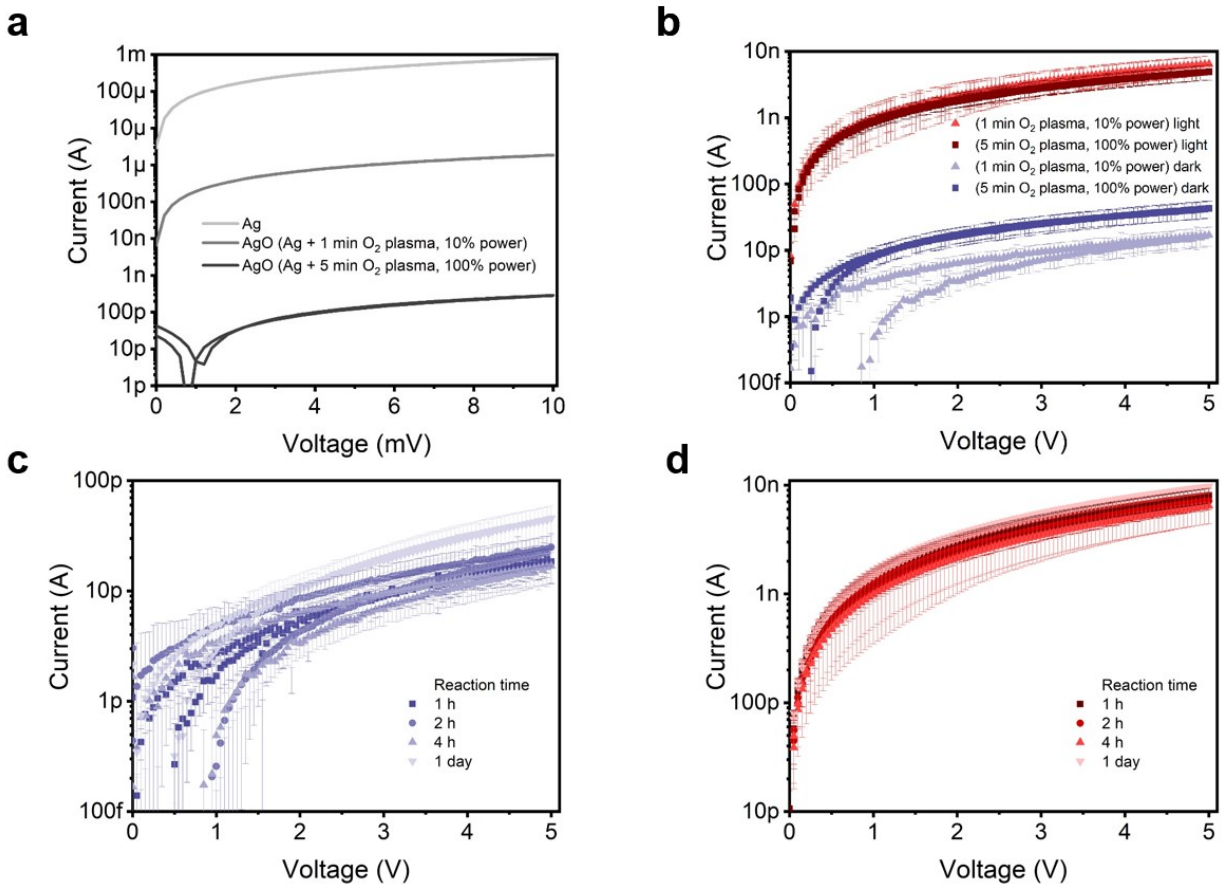

Figure S6. a, Electrical characterization of precursors thin films, reported as IV curves over 5 μm channel: Ag (light grey), AgO by mild plasma oxidation (grey), and AgO by harsh plasma oxidation (dark grey). **b,** IV curves in dark conditions (blues) and under white light illumination (reds) for $[AgSePh]_\infty$ films obtained from mildly (triangles) or harshly (squares) oxidized silver. **c-d,** IV curves in dark conditions **(c)** and under white light illumination **(d)**, for $[AgSePh]_\infty$ NC films, grown 1 h (squares), 2 h (circles), 4 h (upward triangles), and 1 day (downward triangles). Error bars represents the statistical dispersion of results across 4 different devices on the same NC film.

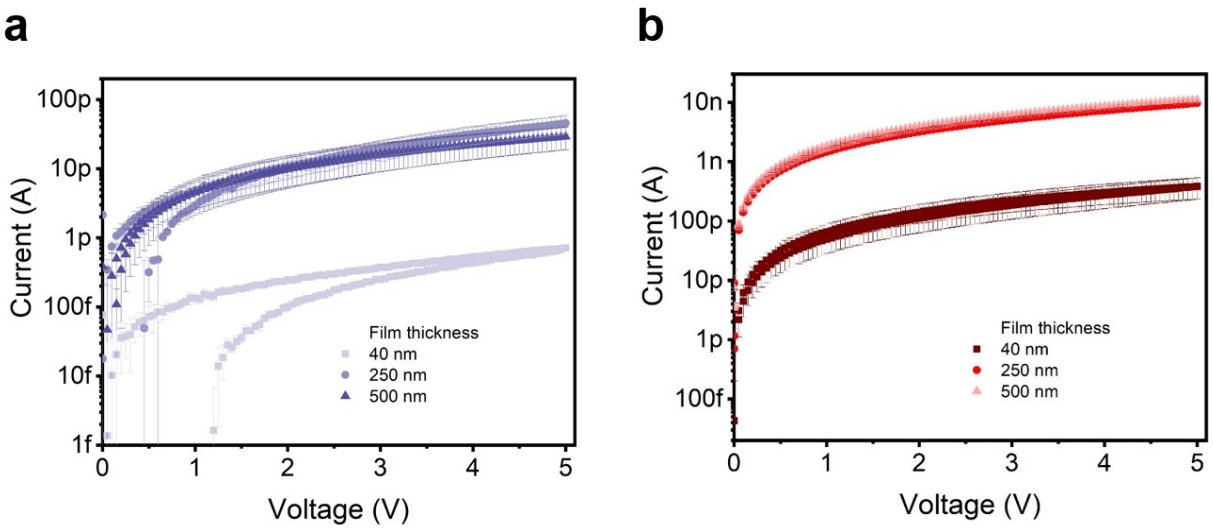

Figure S7. IV curves for different film thicknesses (40 nm – squares, 250 nm – circles, 500 nm – triangles) of the NC film in dark conditions **(a)** and under while light **(b)**. The different NC films where obtained starting from respectively from 5, 20, 50 nm of silver thin films. For a starting Ag film equal or thicker than 20 nm the reaction lead to continuous NC films,[1] resulting in similar dark and photo-current characteristics. Error bars represents the statistical dispersion of results across 4 different devices on the same NC film.

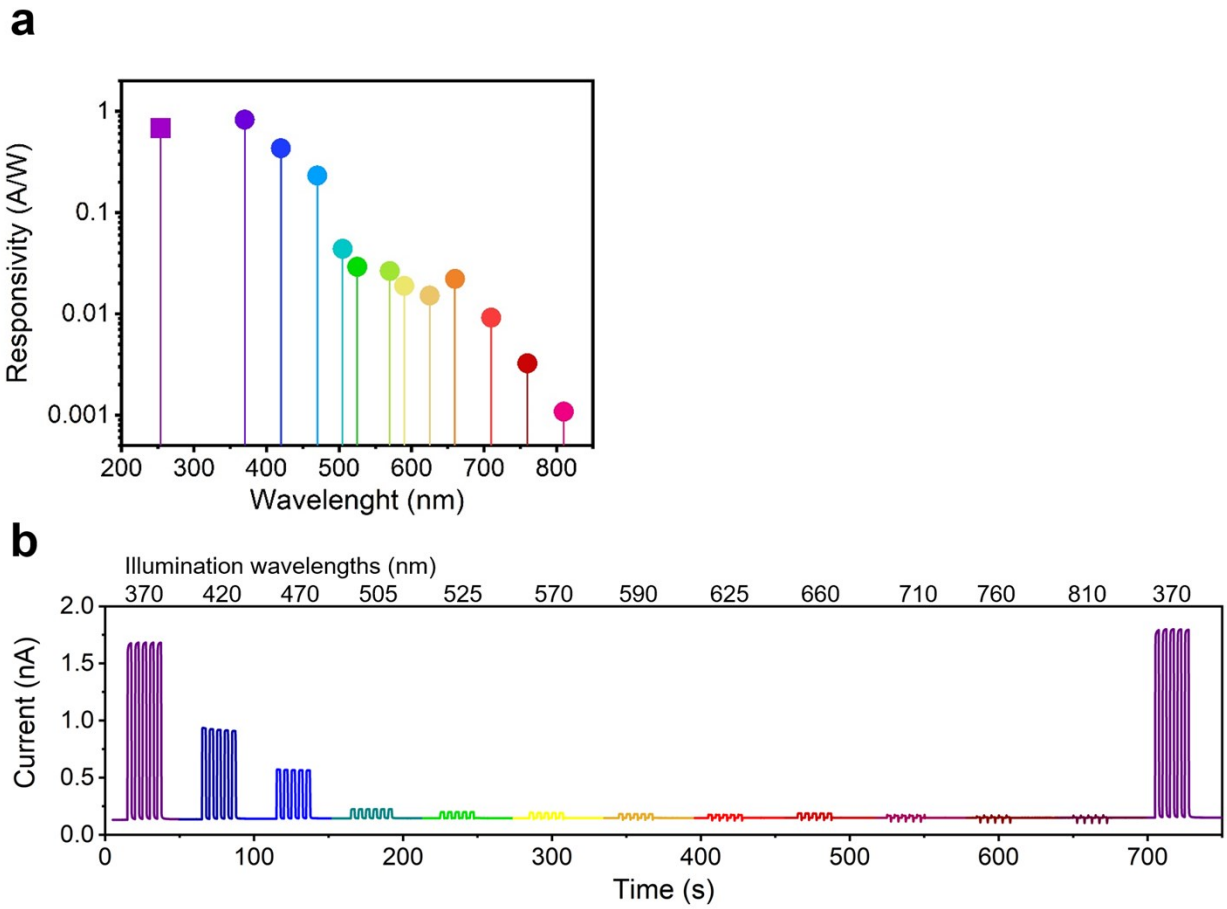

Figure S8. a, Device responsivity over wavelength of the incidence light, in log units. The illumination was provided by LEDs (circles) and a 254 nm lamp (square). **b,** Raw data of modulated photocurrent acquired over time with different monochromatic illuminations (LEDs) used for calculating the sensor responsivity. The deep UV data-point (254 nm wavelength) was acquired separately as no modulation could be performed.

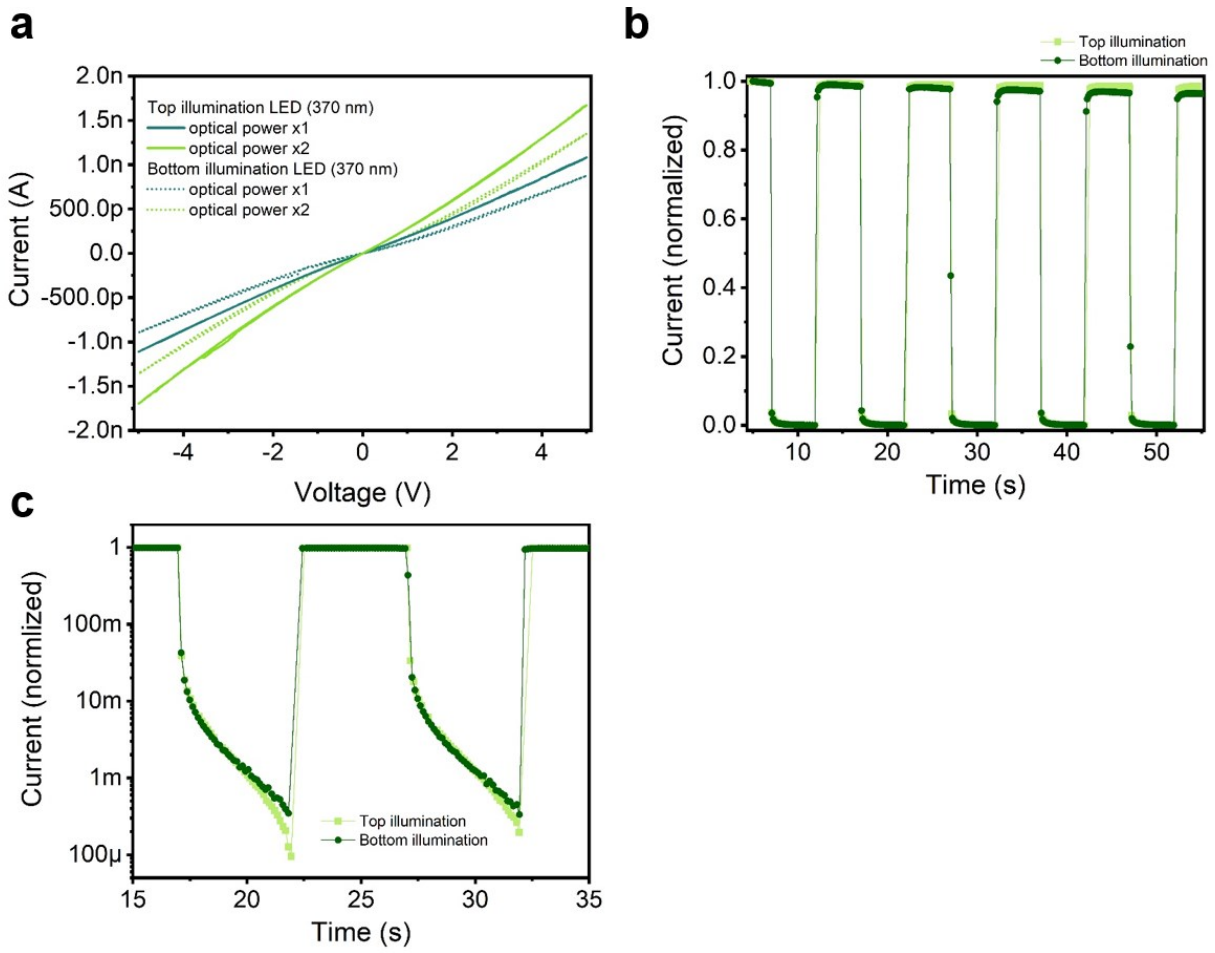

Figure S9. NC films photo-response for top and bottom illumination. a, IV characteristics under two illumination photon flux intensities (1x and 2x) for top (solid line) and bottom (dotted line) illumination, showing very similar behaviour. Indeed, the direct comparison of the absolute photo-current values are difficult since the experimental conditions did not allow for the exact same light intensity onto the sample area. Nevertheless, the normalized photo-current variation over time for cyclic switching (ON/OFF) of the 370 nm LED **(b,c)** shows no clear difference for top/bottom illumination, even at closer look (semi-log plot, zoomed **(c)**).

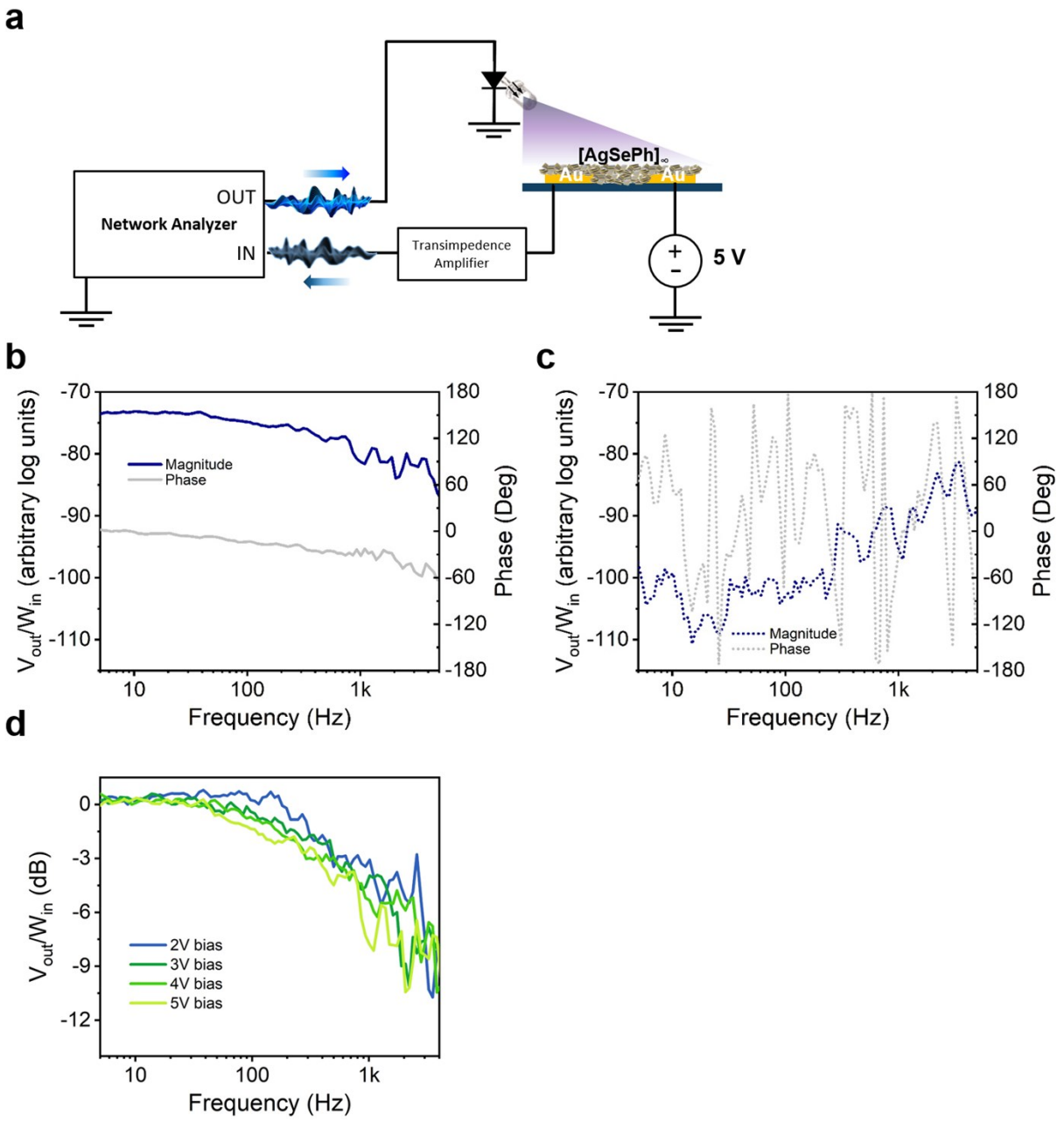

Figure S10. a, Scheme of the instrumental apparatus used for detection of the frequency-dependent photo-generated current. **b,** Typical frequency response of the UV sensor (see Figure 5 in the main text for detailed description) and its reference **(c)**, obtained by inserting a shutter in front of the LED to check no electromagnetic coupling between the light generation and the photo-generated signal returning to the network analyser. **d,** Normalized device frequency response

obtained for four different voltage biased applied to the electrodes. The cut-off frequency does not change.

BIBLIOGRAPHY

(1) Maserati, L.; Pecorario, S.; Prato, M.; Caironi, M. Understanding the Synthetic Pathway to Large-Area, High-Quality [AgSePh]∞ Nanocrystal Films. *J. Phys. Chem. C* **2020**, *124* (41), 22845–22852.